Journal of Magnetic Resonance 204 (2010) 37–49

Contents lists available at ScienceDirect

Journal of Magnetic Resonance

journal homepage: www.elsevier.com/locate/jmr

Magnetized boxes for housing polarized spins in homogeneous fields

S. Hiebel [1,2], T. Großmann [1,3], D. Kiselev [1,4], J. Schmiedeskamp [1,5], Y. Gusev [6], W. Heil, S. Karpuk, J. Krimmer, E.W. Otten *, Z. Salhi

Institut für Physik der Johannes Gutenberg-Universität Mainz, D-55099 Mainz, Germany

ARTICLE INFO

Article history:
Received 28 July 2009
Revised 16 January 2010
Available online 14 February 2010

Keywords:
Magnet design
Relaxation by field gradient
Polarized gas transport
MRI

ABSTRACT

We present novel types of permanently magnetized as well as current powered boxes built from soft-ferromagnetic materials. They provide shielded magnetic fields which are homogeneous within a large fraction of the enclosed volume, thus minimizing size, weight, and costs. For the permanently magnetized solutions, homogenization is achieved either by an optimized distribution of the permanent field sources or by jacketing the field with a soft-ferromagnetic cylindrical shell which is magnetized in parallel to the enclosed field. The latter principle may be applied up to fields of about 0.1 T. With fields of about 1 mT, such boxes are being used for shipping spin-polarized ^{3}He worldwide for MRI purposes.

For current powered boxes, we present concepts and realizations of uniaxial and tri-axial shielded magnetic fields which are homogeneous on the level of 10^{-4} within the entire shielded volume. This is achieved by inserting tightly fitting solenoids into a box from soft-magnetic material. The flexible tri-axial solution suits in particular laboratory applications, e.g. for establishing a spin quantization axis.

1. Introduction

Experimental and technological tasks often require the provision of a homogeneous magnetic field under conditions where external stray fields may interfere, or restrictions in total space may demand a compact configuration, or simply size, weight and costs of the magnetic setup shall be optimized. Our team has been confronted with such problems in the course of handling and storing samples of polarized ^{3}He gas more or less free of relaxation [1] which among other precautions requires a homogeneous magnetic guiding field. This so called hyperpolarized gas may feature a nuclear spin polarization degree of up to 80%, i.e. many orders of magnitude above the usual Boltzmann equilibrium. This is achieved by spin exchange (SEOP) or metastability exchange (MEOP) techniques of optical pumping [2–5]. Hyperpolarized ^{3}He serves as a nuclear reaction target [6], as a neutron spin filter [5,7,8], or as a contrast agent in magnetic resonance imaging [9–11], to name just a few prominent applications pursued by numerous groups worldwide. For these purposes we have developed several types of boxes, called "spin boxes", which are built from magnetically soft material. Their design aims at: (i) shielding external stray fields; (ii) maximizing the filling factor F, defined as the ratio of the volume V_{hom}, wherein the magnetic field is sufficiently homogeneous and the total accessible box volume V_{tot}:

$$F = V_{\mathrm{hom}}/V_{\mathrm{tot}}. \quad (1)$$

The boxes are magnetized either by permanent magnets or by specially designed current coils. Permanently magnetized solutions are preferred for storage and transport purposes when the gas has been polarized, e.g. at an off-line facility, and then has to be shipped to customers elsewhere [12,13]. Fig. 1 shows a photo of the permanently magnetized spin box mark 3 (Section 3.3); the top cover is removed to show inside three flasks of 1.1 liter volume each, filled with hyperpolarized ^{3}He at a pressure of 2.7 bar, which is the upper limit for ordinary airfreight.

In an experimental situation, on the other hand, one likes the flexibility of a current driven solution: It may allow tuning and turning the field or it may provide openings in the box which still conserve the homogeneity of the field inside by adapting the current tracks accordingly.

Some of these devices have already been used by our group for several years but so far have been mentioned only shortly in publications featuring a different focus. In the present paper we treat their physics and techniques in a systematic context. In addition, we present here a totally novel concept of homogenizing a magnetic field rather globally, namely by jacketing it with a cylindrical shell of highly permeable material which is magnetized in the

* Corresponding author. Fax: +49 6131 3925179.
E-mail address: ernst.otten@uni-mainz.de (E.W. Otten).

[1] The paper comprises parts of the doctoral theses of Stefan Hiebel, Tino Großmann, Daniela Kiselev and Jörg Schmiedeskamp.

[2] Present address: Sekels GmbH, Ober-Mörlen, Germany.
[3] Present address: AOK, Bad Homburg v. d. H., Germany.
[4] née Rohe, Present address: Paul Scherrer Institute, Villigen, Switzerland.
[5] Present address: SIEMENS Medical Solutions, Frankfurt, Germany.
[6] Present address: St. Petersburg Nuclear Physics Institute, Gatchina, Russia.

1090-7807/$ - see front matter © 2010 Elsevier Inc. All rights reserved.
doi:10.1016/j.jmr.2010.01.017

Fig. 1. Permanently magnetized spin box mark 3 for shipping hyperpolarized ^{3}He (Section 3.3). On the right leans the top cover which forms the second pole face, on the left the respective clamp ring. Inside one recognizes three flasks of 1.1 liter volume each, filled with hyperpolarized ^{3}He at a pressure of 2.7 bar and closed by a stop cock. A cover from flexible tissue protects the user from glass splinters in the case of bursting. The magnetic field is 0.8 mT. Within the volume occupied by the flasks, the relative field gradient is limited to $\lesssim 10^{-3}$/cm when the box is closed.

same direction as the enclosed field (Section 2.3). The various concepts are presented on the basis of two-dimensional simulations using the fast FEM program *femm 4.0*, © 1998–2003 by D. Meeker.

Preserving the spin polarization of a gas requires a homogeneous rather than a strong guiding field, in order to ensure an adiabatic field change with respect to the spin motion along the fast diffusion path. Consequently the gradient relaxation rate $1/T_{1G}$ turns out to be just the product of the diffusion constant D and the averaged square of the *relative* transverse field gradient $\left\langle \boldsymbol{G}^2_{\perp \mathrm{rel}} \right\rangle$ [14–17]:

$$1/T_{1G} = D\left\langle \boldsymbol{G}^2_{\perp \mathrm{rel}} \right\rangle = \frac{D}{B_0^2}\left\langle |\vec{\nabla}B_x|^2 + |\vec{\nabla}B_y|^2 \right\rangle \approx \frac{D}{B_0^2}\left\langle \left(\frac{\partial B_z}{\partial z}\right)^2 + \left(\frac{\partial B_z}{\partial r}\right)^2 \right\rangle \approx \frac{D}{B_0^2}\left\langle \left(\frac{\partial B}{\partial z}\right)^2 + \left(\frac{\partial B}{\partial r}\right)^2 \right\rangle. \quad (2)$$

The average is taken over the enclosed gas volume with $B_0 = B_z(0)$ being the central field value aligned along the z-axis. The two approximations on the right side of (2) have been derived for the standard configuration of a nearly homogeneous, axi-symmetric field around a central saddle point (see Appendix). Eq. (2) holds under the following relations between the average diffusion time to the wall τ_{diff} in a vessel of radius R, the Larmor period $1/\omega_{\mathrm{L}}$ and the time between gas kinetic collisions τ_{c}:

$$\tau_{\mathrm{diff}} \approx R^2/D \gg 1/\omega_{\mathrm{L}} \gg \tau_{\mathrm{c}}. \quad (3)$$

Eq. (3) is well fulfilled in the cases of interest here. For our example of a ^{3}He-pressure of 2.7 bar at room temperature, D is about 0.7 cm^2/s [18]. For a design value of the relative gradient being smaller than 10^{-3}/cm the gradient relaxation time takes a lower limit $T_{1G} > 400$ h:

$$\left\langle \boldsymbol{G}^2_{\perp \mathrm{rel}} \right\rangle^{1/2} < 10^{-3}/\mathrm{cm} \underset{D=0.7\ \mathrm{cm}^2/\mathrm{s}}{\rightarrow} T_{1G} > 400\ \mathrm{h}. \quad (4)$$

This limit seems reasonable in view of the two other ^{3}He-relaxation mechanisms at work, namely: (i) dipolar relaxation with $T_{1D} = 300$ h at 2.7 bar and 300 K [19], (ii) relaxation at the containment wall. For the latter typical values of about 100 h $< T_{1W} <$ 250 h are routinely reached nowadays using demagnetized alumino silicate glass [1,20].

Since only the relative gradient matters in (2) low magnetic fields in the range of $B_0 \approx 1$ mT are chosen for reasons of cost and convenience. For other purposes, however, the solutions which we present here may be scaled up to much higher fields of up to 0.1 T.

This paper is organized as follows: in Section 2 we discuss principles of permanently magnetized spin boxes and numerical design studies, followed in Section 3 by their technical realizations and the results obtained. In the same sense Sections 4 and 5 deal with current powered boxes. Conclusions are given in Section 6.

2. Design studies of homogeneous permanent magnetic fields

Textbook examples of homogeneous magnetic fields are long solenoids or magnets with closely spaced parallel pole faces. There the inhomogeneous regions near the boundaries are simply pushed far out by the extreme aspect ratio. More practical aspect ratios of homogeneous fields are obtained by means of correction coils or shims which compensate field gradients in the center up to higher orders and form an extended, flat saddle point region there. In low field applications, such as our spin boxes, one faces in addition the danger of spoiling the homogeneity by external stray fields; this requires magnetic shielding. In the following we will present several design studies for the construction of shielded permanent magnetic fields with special emphasis to achieve a maximum fraction F of useful homogeneous field volume (see (1)) with minimal size, weight and cost. Since we check and optimize our concepts by fast two-dimensional FEM field simulations using *femm 4.0*, we usually choose axially symmetric configurations in order to reduce the mathematical dimension of the problem by one.

2.1. Simple, shielded field box magnetized by permanent magnets

A straight forward realization of a shielded, permanently magnetized field box would consist just of an axially symmetric, closed cylinder of radius R and length L from a material with high magnetic permeability μ such as mu-metal, for example. Fig. 2a shows a schematic cross-section of such a pot-like box; it may be magnetized by inserting between the yoke and the pole faces two rings with radius R and width d which are permanently magnetized along the z-axis with a remanent field B_{R}.

They provide a remanent magnetic flux Φ_{R}. If we neglect for the moment the demagnetizing factor of the ring profile as well as stray fields, Φ_{R} equals the flux inside the box Φ_{box} yielding the estimates:

$$\Phi_{\mathrm{R}} \approx 2\pi R d B_{\mathrm{R}} \approx \Phi_{\mathrm{box}} \approx \int_{\text{box cross-section}} \vec{B}_{\mathrm{box}} \cdot \mathrm{d}\vec{A}. \quad (5)$$

Due to their high permeability μ, the front plates act as pole faces presenting flat magnetic equipotential surfaces which support homogeneity inside. The magnetic potential difference ΔV_H in-between is set up by the two permanently magnetized rings in series. It equals the path integral along the magnetizing field $H = B/\mu\mu_0$ (with the magnetic field constant $\mu_0 = 4\pi \times 10^{-7}$ Tm/A) inside the box of length L:

$$\Delta V_H = \int_0^L \vec{H}_{\mathrm{box}} \cdot \mathrm{d}\vec{s}. \quad (6)$$

The cylindrical shell acts as a magnetic yoke closing the magnetic flux. If the mu-metal is magnetized well below saturation, the shielding property of the box will still be intact, at least in the dangerous transverse direction (see Section 3.1). Fig. 3a shows the calculated B-field inside such a box in a false color code which

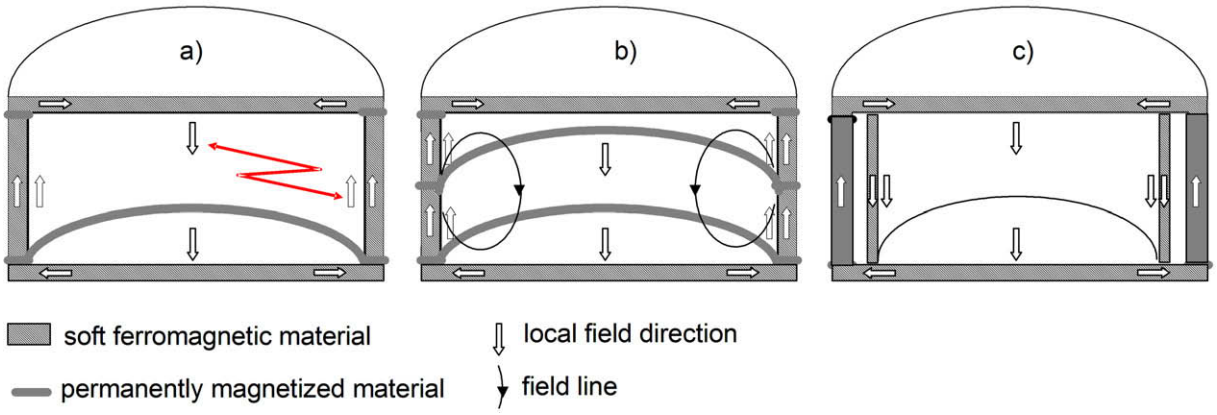

Fig. 2. Different schemes of shielded, permanently magnetized pot-like magnets. (a) Simple solution with field sources placed between pole faces and yoke; the field reversal near the yoke causes a strong field inhomogeneity inside. (b) Like (a) but with an additional permanent field source in the central plane which compensates the field decrease in radial direction observed in (a). (c) With a field shaping shell inside, magnetized parallel to the central field.

stretches over ±10 steps of height $\Delta B/B_0 = 5 \times 10^{-4}$ around a central field value of $B_0 = 0.535$ mT. Pole faces **1** and shell **2** are 1 mm thick. Their relative permeability is fixed to $\mu = 10^5$ which is about the peak value reached by mu-metal. The rings **3** have a cross-section of 1×1 mm^2 and are remanently magnetized at $B_R = 1.15$ T. The inner dimensions, chosen as $R = 20$ cm, $L = 18$ cm, form a comfortable aspect ratio $L/R \approx 1$. But the homogeneity is quite unsatisfactory, missing criterion (4) already on the first cm around the central saddle point.

2.2. Compensation of field gradients by optimized distribution of permanent field sources

The problem of the simple field box described above originates from the unfavorable boundary condition presented by the shell where the steadily continuing tangential H-field produces a magnetic flux at the inner surface which is oriented *opposite* to the one in the center. In the best case, i.e. $\mu \to \infty$, this field just vanishes. Thereby the field is forced to decline rapidly in radial direction unless a much smaller aspect ratio is chosen. This gradient may be compensated in a simple manner by choosing an optimized distribution of permanent field sources: if we split, for instance, the shell in the central plane and place a third permanently magnetized ring into the gap, we introduce a step of magnetic potential also between the two halves of the shell which is bridged inside by magnetic field lines (Fig. 2b). In the neighborhood of the central plane, these additional field lines are aligned parallel to the central field and can compensate its radial decline [21]. In the simulation of Fig. 3b we therefore added a third, equally magnetized 2.2 mm high ring **4** in the middle of the shell which has been optimized to compensate the leading second order in the central saddle point region.

The field plot shows that $\boldsymbol{G}_{\perp \mathrm{rel}}$ remains below the critical level of 10^{-3}/cm up to a radius of $r_h \approx 11$ cm as may be read from the width of the color steps. The corresponding filling factor (1) is $F = 30\%$. Beyond this homogenized plateau we recognize a typical steep transition to higher field gradients. The realization of this concept is described in Section 3.1.

2.3. Forming a homogeneous magnetic field by a field shaping, parallel magnetized shell

Instead of shimming the magnetic field locally, let us try to conceive a configuration which yields *global* homogeneity inside a shielding box – at least in the ideal case: consider, for instance, a closed cylinder with inner radius R and thickness d, built from soft-ferromagnetic material with permeability μ which is magnetized by a surrounding, permanently magnetized shell as shown schematically in Fig. 2c. Again the permanent magnet provides a certain magnetic potential (6) between the pole faces of the cylinder. But its flux Φ_R (5) is now *shared* between the inner cylinder volume and the shell of the box in the *same* direction. If we neglect the stray flux out of the shell, the continuity of the tangential component of H across the boundary and the cylindrical shape of the whole box will establish the relations

$$H_{\uparrow\uparrow \mathrm{in}} = H_{\uparrow\uparrow \mathrm{out}} = H = \mathrm{const}, \tag{7}$$

where the magnetizing fields in the enclosed volume as well as along the inner shell are given by

$$H = \frac{\Phi_R}{\mu_0 \pi (R^2 + 2\mu R d)}. \tag{8}$$

Under these assumptions the field inside would be globally constant, indeed, since any equipotential surface is just a cross-section parallel to the pole faces [22,23].This situation is analog to an electric field between parallel plates which are connected by a conducting, homogeneous cylindrical shell. A numerical simulation of this configuration is shown in Fig. 3c with the input parameters $R = 20$ cm, $L = 18$ cm, $d_1 = d_5 = 1$ mm, $\mu = 10^5$, $\Phi_R = 17.3$ Tcm^2. Except for the very corner, the simulated field inside is quasi homogeneous all over, as expected. But the H-field has dropped to 11 A/m ($B = 14$ μT) since the high μ of the shell acts as a shunt which short circuits the magnetic flux. The same value is derived from (8) which applies here nicely since the high μ prevents almost any stray flux.

In order to achieve satisfactory field values, however, the permeability of the shell has to be lowered. On the other hand this measure causes an enhancement of the stray flux as well as a decline of the shielding factor. The numerical consequences are shown in the simulations of Fig. 3d. There we repeated the simulation for this configuration with a field shaping shell **7** from ARMCO soft iron, whereas the pole faces are still from mu-metal. For both materials their initial magnetization curves as given in [24] and [25], respectively, have been entered into the calculation. The permanently magnetized shell **6** is chosen from AlNiCo with a demagnetization curve as given in [26]. By reduction of permeability in the field shaping shell (down to $\mu \approx 2500$) the central field grows to $B_0 = 0.4$ mT which is in the region of interest. However, due to the stray flux out of the field shaping shell, the tangential field component (7) is not constant anymore and we observe a drop of field strength of about 5% along the shell towards the central plane.

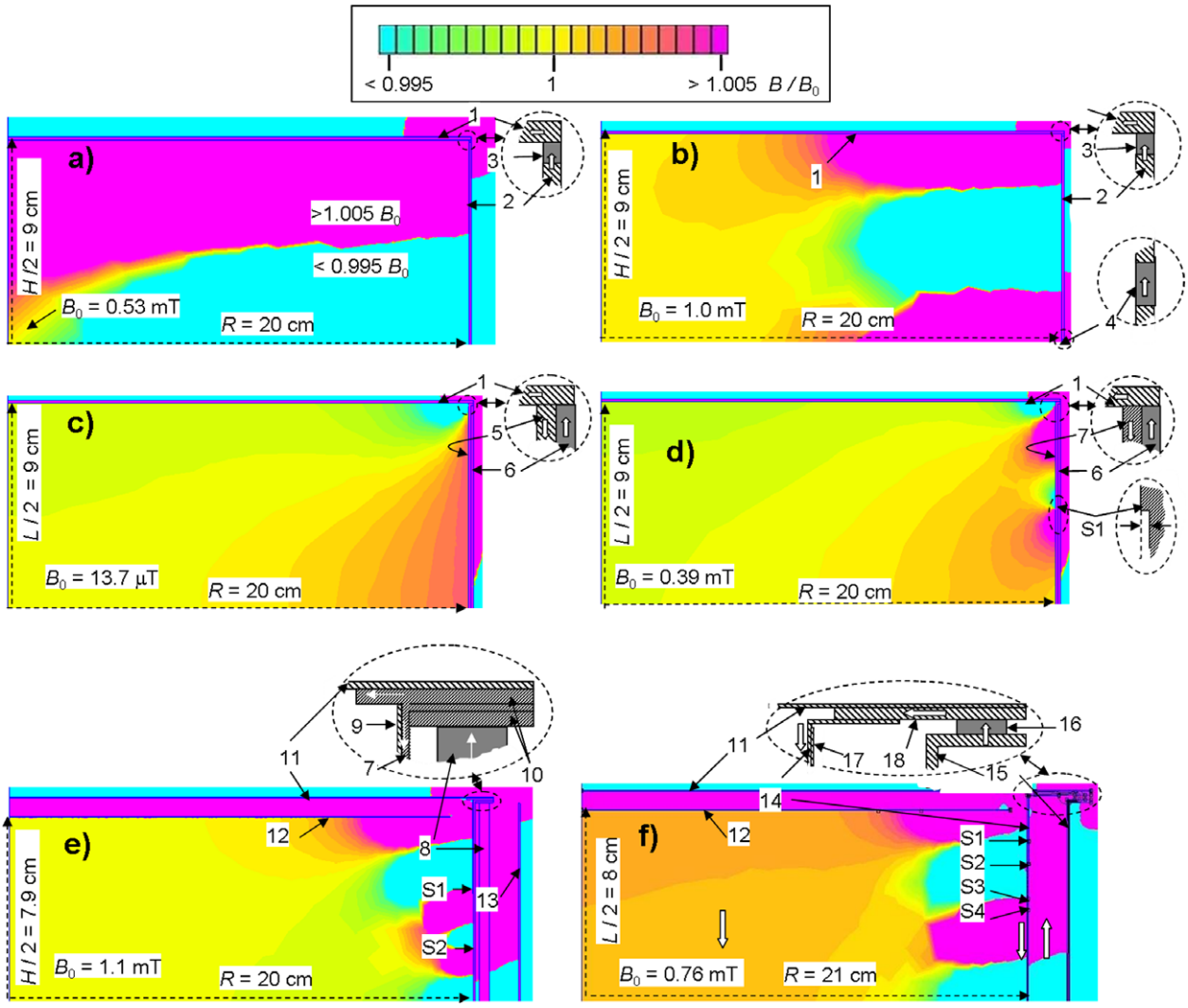

Fig. 3. Two-dimensional simulation of magnetic fields within various types of permanently magnetized boxes. The false color code is graded in steps of 0.5‰ of the central field value B_0. Because of axial symmetry, only one quadrant of the total cross-section is shown. (a) Simple, non-homogenized box; **1** = pole face, **2** = yoke and shield, both at $\mu = 10^5$ = const., thickness $d_1 = d_2 = 1$ mm, **3** = remanently magnetized ring at $B_R = 1.15$ T = const. (b) Like a) but with an additional permanent field source **4** in the middle of the yoke. (c) Box with inner, field shaping shell **5** at $\mu = 10^5$ = const. and outer, remanently magnetized shell **6** ($B_R = 1.15$ T = const.); $d_5 = 1$ mm, $d_6 = 1.2$ mm. (d) Like (c) but simulated with realistic magnetization curves for the mu-metal pole faces **1**, the remanently magnetized shell **6** from AlNiCo 500 and the field shaping shell **7** from ARMCO soft iron; $d_7 = 1$ mm, step S1 = 7 µm. (e) Field simulation applying to prototype mark 2; **8** = AlNiCo rods, **9** = shimming mu-metal foils forming steps S1 = 200 µm, S2 = 50 µm, **10** = ARMCO rings, **11** and **12** = double pole faces from mu-metal, **13** = mu-metal shield. (f) Field simulation applying to prototype mark 3; **14** = field shaping shell from mu-metal, **15** = mu-metal yoke and shield, **16** = magnetic rubber ring, **17** = shimming mu-metal foils, forming steps S1 = 0.1 mm, S2 = 0.1 mm, S3 = 0.1 mm, S4 = 0.05 mm. **18** = connecting ring from mu-metal.

Still the homogeneity criterion (4) is fulfilled up to a radius of $r_h = 13$ cm.

2.4. Compensation of the stray flux effect by shimming the field shaping shell

The field homogeneity as controlled by condition (7) may be restored, in principle, if we compensate the stray flux out of the field shaping shell by a corresponding reduction of its solid cross-section so that the flux density inside the shell and hence also $H_{\uparrow\uparrow in}$ are kept constant [22,23]. By this kind of shimming, a full compensation of the stray flux effect seems to be feasible at first sight. This conception is partly spoiled, however, by the fact that stray flux lines running inside the box necessarily give rise to some inhomogeneity through their curvature. Still the idea of shell shimming works rather well as shown by the field simulation in Fig. 3d. There the thickness of the central section of the field shaping shell **7** was reduced by 7 µm in a single step. Criterion (4) is now fulfilled up to a radius of $r_h = 18$ cm, corresponding to a usable filling factor (1) of 80%. The result may be improved somewhat further by a finer step grading or even a continuous tapering of the shell waist. But still one observes unsatisfactory homogeneity in a residual, peripheral zone which grows with decreasing permeability and thickness of the field shaping shell.

2.5. Reinforcement of shielding by an additional outer shell

The considerations and simulations presented in this and the next section apply to the actual design of the two prototypes mark 2 and mark 3 (Sections 3.2 and 3.3) which have been built to verify our ideas about a field shaping shell by experiment. Since this shell has to be magnetized close to saturation it does not shield off external stray fields safely any more. Hence we added in the simulation of Fig. 3e (applying to mark 2) an outer shell **13** from mu-metal of radius $R = 22$ cm and 0.5 mm thickness. In order to improve the homogeneity, we have split, moreover, the pole faces

into two sheets of mu-metal (**11** and **12**), 0.5 mm thick and 1.2 cm apart. The magnetic flux is lead from the permanent source **8** onto the outer ones. The spacing between the two sheets forms a magnetic resistance which equalizes the flux density across and hence yields a better equipotential surface on the inner pole face which is a well known effect. The permanent field source **8** of mark 2 consists of 36 rods from AlNiCo 500, 17 cm long and 5 mm in diameter. For our 2D simulation their total flux of 8 Tcm^2 had to be averaged over the full azimuth. The magnetic conductance around the pole faces of the permanent magnets was reinforced by bending the edges of the inner, field shaping shell outwards by 90° and covering them with 1 mm thick ARMCO iron rings **10** from both sides.

In order to increase the field inside the box further, as well as for reasons of weight, the thickness of the field shaping shell **7** was reduced to 0.5 mm. Thinning the field shaping inner shell as well as adding the outer shield enhances the stray flux considerably which requires more careful shimming. The simulation considered shimming by addition of mu-metal foils **9** onto the field shaping shell. They form two steps of depth S1 = 200 μm and S2 = 50 μm, respectively. The resulting field distribution shows that criterion (4) is fulfilled up to a radius of 17 cm, corresponding to a filling factor (1) of $F = 70\%$.

2.6. All mu-metal spin box with an inner, field shaping shell and a shielding yoke

It is clear that ultimate performance in the low field regime cannot be expected using ordinary soft iron; its rather high coercive field strength which may vary between 12 and 160 A/m according to Ref. [27] gives rise to perturbing remanent magnetization. Therefore, we present in this section an alternative design, making use of mu-metal only. The choice of a field shaping shell from mu-metal requires to drive its magnetization to saturation occurring at $B_S \approx 0.7$ T already and to lower the permeability down to $\mu \approx 700$ in order to achieve a field around 1 mT inside the box. Correspondingly the magnetic stray flux increases and requires more careful shimming. Hence other soft-magnetic materials with low coercive force but higher saturation magnetization might do an even better job. On the other hand, mu-metal is a well established material in low field applications, and the simulations as well as the realization of this concept by mark 3 (Section 3.3) turned out to meet the goal.

Regarding the design of the permanent field source and the mu-metal shield, we tried this time a solution similar to Fig. 2a: As shown in Fig. 3f, two rings **16** (2 mm high, 4 mm wide) cut from strontium ferrite loaded rubber foil with a remanent magnetization of $B_R = 0.24$ T [28] have been placed between a yoke from mu-metal **15** and two connecting rings **18**. The latter transfer the magnetic flux onto the outer pole faces **11** and the field shaping shell **14** in parallel. In order to avoid saturation in the yoke; its wall thickness has been enhanced to 1.5 mm. Like in the case of mark 2, the pole faces are split into an outer **11** and an inner plate **12**. Pole faces and field shaping shell are cut from 0.5 mm thick mu-metal sheets. The field is homogenized by wrapping mu-metal foils **17** around the field shaping shell, forming shimming steps S1–S4. The simulation meets criterion (4) up to a radius of 16 cm out of 21 cm, corresponding to a filling factor of $F \approx 60\%$.

3. Realizations of permanently magnetized spin boxes

In this chapter we report on three dedicated realizations of permanently magnetized, shielded spin boxes following the concepts of Sections 2.2, 2.5, 2.6. The first and the third version have been produced in a small series and are being used for shipping hyperpolarized ^{3}He to our partners worldwide, particularly within the European networks PHIL [29] and PHELINET [30].

3.1. Spin box with optimized distribution of permanent field sources (mark 1)

The first permanently magnetized spin box we built was a prototype homogenized by optimized distribution of field sources (Section 2.2) [21,31]. Here we report on a later version (mark 1) [32] which is still in use. The free dimensions inside are $R = 30$ cm, $L = 22$ cm. It weighs 17.5 kg. Pole faces and shell are made from 0.5 mm thick mu-metal sheets (see Fig. 4a). The pole faces are split into an outer and an inner sheet for improving the homogeneity as described in Section 2.5. Both sheets are glued onto a 12 mm thick honeycomb structure which guarantees flatness and mechanical stability. For the latter reason, also the mu-metal shell is covered by an aluminum sheet with solid foam filled into the spacing in-between. The shell is split in the middle plane where the box can be opened for loading.

Permanent magnets are placed between the outer pole faces and the shell as well as into the gap between the two halves of the shell. They were cut from a commercially available, 2 mm thick foil of magnetic rubber, magnetized transversely at $B_R = 0.24$ T. The individual pieces were distributed equally over the azimuth. The ratio of the number of magnets placed on the pole faces to that in the middle plane has been varied until a field plateau of optimal homogeneity and width was found. Measurements were performed with a fluxgate sensor (Bartington MAG-03MS, resolution better than 0.1 μT, range ±1 mT). Fig. 4b shows the radial profile of the relative radial derivative of the axial field B_z, measured for

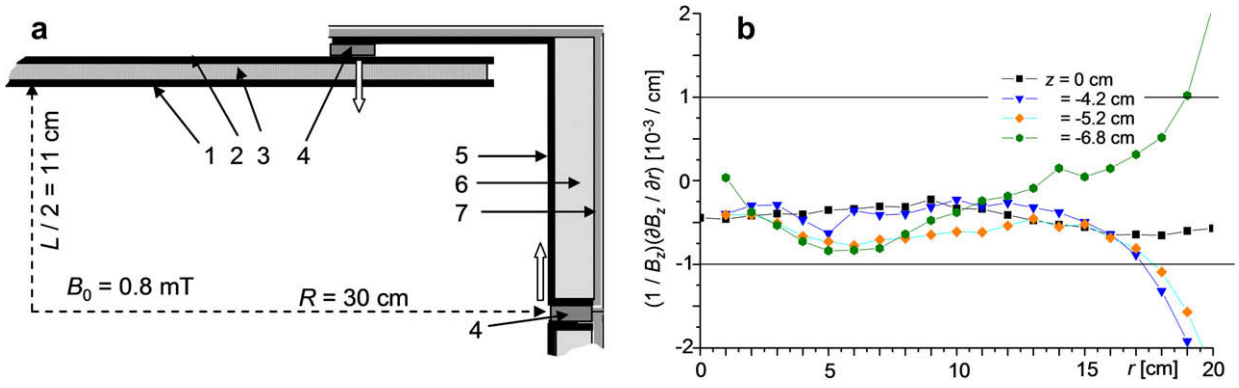

Fig. 4. (a) Quadrant of the cross-section of spin box mark 1: 1 = inner pole face, 2 = outer pole face, 3 = honeycomb structure, 4 = magnetic rubber, 5 = yoke and shield, 6 = solid foam, 7 = aluminum cover. (b) Relative radial derivative of the axial field B_z as a function of radius, measured in mark 1, No. 3 at four different distances z from the middle plane. The errors are dominated by inaccurate positioning of the sensor (approx. 2 mm). The lines between the symbols are guides for the eyes only.

one out of the six spin boxes built [32]. The corresponding axial derivative has not been measured explicitly. Since its size is found to be about equal in similar cases we may estimate that the total relative transverse field gradient in (2) is larger by $\sqrt{2}$ than shown in the plots. Criterion (4) is then slightly exceeded locally within the aspired storage volume. The plots vary somewhat within the series of six boxes built. The radius at which $\boldsymbol{G}_{\perp\mathrm{rel}}$ starts to rise steeply beyond the 10^{-3}/cm level, ranges from 14 to 18 cm. This corresponds to filling factors (1) between 22% and 36%. The boxes house three of our 1.1 liter ^{3}He-flasks. Frequent exposure to harsh handling when shipping has slightly dented them during years of service. But with some treatment we still keep the gradient relaxation time at a tolerable level of $T_{1\mathrm{G}}(20\,^\circ\mathrm{C}, 2.7\ \mathrm{bar}) \geqslant 100$ h.

The shielding factor S of a closed box can be roughly estimated by the formula [25]

$$S = B_{\mathrm{out}}/B_{in} \approx (\mu \cdot t/d) + 1, \tag{9}$$

where t is the wall thickness and d is the room diagonal. In axial direction S has been measured to be as small as $S_{\uparrow\uparrow} = 4$ due to the 2 mm slits in the equatorial plane as well as between the shell and the pole faces. But this does not harm, because the penetrating field is homogenized by the pole faces and simply added to the internal field in parallel. In the harmful transverse direction, however, a satisfactory value of $S_\perp = 90$ has been measured. From (9) one would estimate a corresponding permeability of $\mu = 110\ 000$ which ranges at the upper end of reported values [25]. At this point one should mention that these mu-metal components have been properly annealed after machining and welding.

A recent publication [33] describes a spin box whose design is based on a variant of the principle of optimized distribution of field sources, originally described in [21]. It is designed as an elongated cuboid with free access from two open sides and is meant for transporting polarized ^{3}He cells within a laboratory.

3.2. Prototype of a spin box with parallel shell magnetization (mark 2)

The idea of homogenizing a magnetic field by parallel shell magnetization has been realized for a prototype according to the design presented in Section 2.5 and Fig. 3e [22]. The two-layer pole faces **11**, **12** as well as the two shells **7**, **13** were mechanically reinforced by gluing honey comb structures from polycarbonate in-between. The box is opened by removing either of the pole faces. The box weighs 15 kg and is easier to handle than mark 1 due to saving a factor of 2 in overall volume. For this mere feasibility study we have accepted some compromises in the choice and treatment of magnetic components such as the choice of ARMCO soft iron and the lack of annealing. This should be kept in mind in assessing the experimental results below.

The field gradient was diminished by attaching appropriate layers of annealed mu-metal foils **9** onto the inner surface of the field shaping shell **7**. The resulting optimal profile of shimming was found to be somewhat steeper than in the simulation of Fig. 3e. The residual azimuthal field asymmetry (obviously caused by some remanent magnetization of the soft iron shell) was removed to a satisfactory level by fixing some additional pieces of shimming material onto the shell **7** at places of enhanced field. Fig. 5a shows a field scan along a diameter close to the central plane, taken after shimming [22]. The central plateau stretches out to a radius of about 14 cm. Its field value of 0.8 mT falls somewhat below the calculated 1.1 mT (Fig. 3e). The slight residual asymmetry of the plateau gives rise to an additional radial gradient $\gtrsim 2 \times 10^{-4}$/cm which can be tolerated. Additional scans were performed in order to determine the full relative gradient as defined in (2). The result is shown in Fig. 5b. Beyond a radius of 14 cm, criterion (4) is violated, that is 3 cm below the calculated limit (see Fig. 3e). Still the filling factor of the box is close to 50%.

In order to check the operability of the box, a 1.1 liter flask, filled with 2.6 bar of hyperpolarized ^{3}He was placed at the most eccentric position designed for housing three flasks as shown in Fig. 1 and the relaxation rate was measured online by the steady decrease of an NMR signal as described in [22,32]. The result was $1/T_1 = 0.0098(10)\ \mathrm{h}^{-1}$. Dipolar relaxation at 2.6 bar and room temperature amounts to $1/T_{1\mathrm{D}} = 0.0032(1)\ \mathrm{h}^{-1}$; wall relaxation in this particular flask was measured separately in a strictly homogeneous field yielding $1/T_{1\mathrm{W}} = 0.0031(2)\ \mathrm{h}^{-1}$. Subtracting these two terms the gradient relaxation time in mark 2 was found to be $T_{1\mathrm{G}} \approx 290(83)$ h. This value corresponds to $\left\langle \boldsymbol{G}_{\perp\mathrm{rel}}^2 \right\rangle^{1/2} = 1.2(2) \cdot 10^{-3}\ \mathrm{cm}^{-1}$, showing that the flask already seems to touch the critical rim of the homogenized plateau (Fig. 5b).

The longitudinal and transverse shielding factors were measured to be $S_{\uparrow\uparrow} = 2.7$ and $S_\perp = 23$, respectively. The relatively small values show that the permeability does not reach specified values due to the lack of annealing. In this context we also mention that measuring the shielding factors in an external field of 0.8 mT led to a remanent magnetization of the field shaping ARMCO shell which deteriorated the homogeneity of the shimmed field again. It is planned to rebuild mark 2 using only annealed, soft-magnetic components of low coercivity.

3.3. All mu-metal spin box (mark 3)

The design of mark 3 differs from mark 2 in so far as it features (i) a field shaping shell from mu-metal which is magnetized close to saturation and (ii) a non-saturated, flux returning yoke which acts as a magnetic shield in addition. This design has already been

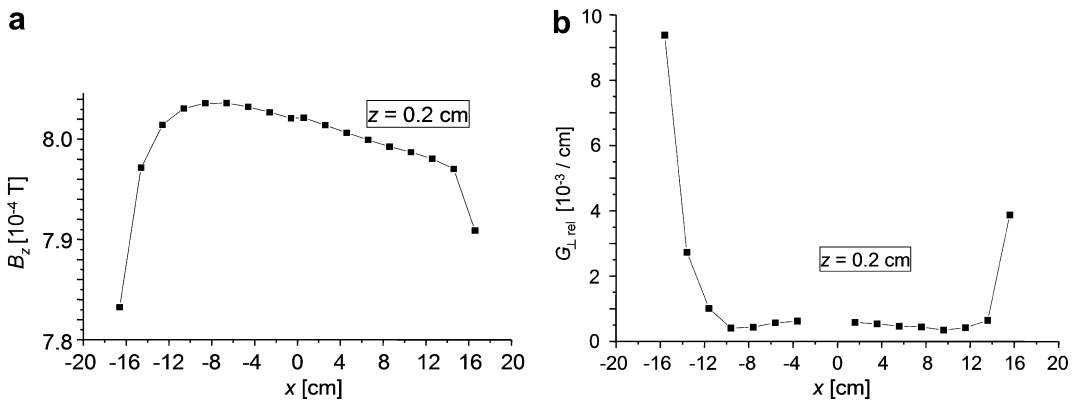

Fig. 5. (a) Scan of the magnetic field component B_z in spin box mark 2 along a diameter close to the central plane. (b) Corresponding transverse relative field gradient as defined in (2). In both diagrams, the errors are dominated by inaccurate positioning of the sensor (approx. 2 mm). The lines between the squares are guides for the eyes only.

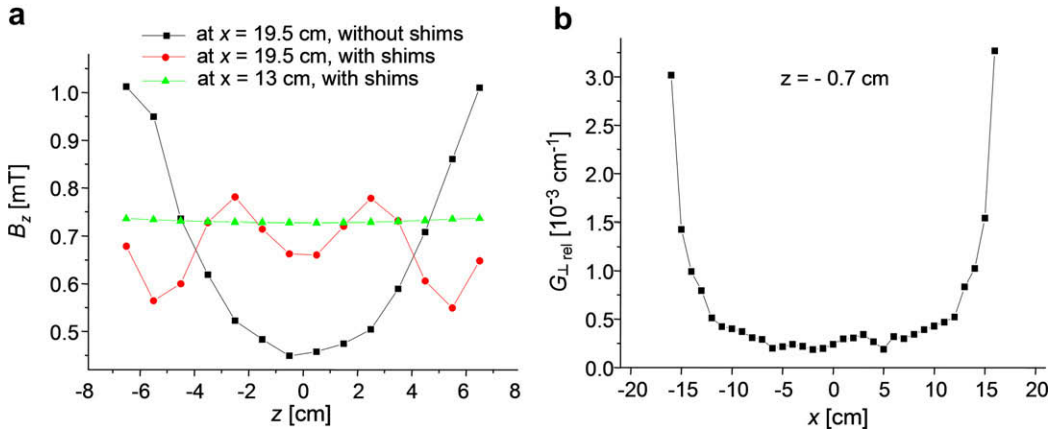

Fig. 6. (a) Scans of the axial field component B_z in spin box mark 3 close to the field shaping shell before (squares) and after shimming (dots), as well as close to the edge of the homogeneous zone (triangles). (b) Transverse relative field gradient as defined in (2), determined along a diameter close to the central plane. In both diagrams, the errors are dominated by inaccurate positioning of the sensor (approx. 2 mm). The lines between the symbols are guides for the eyes only.

tested successfully in a numerical simulation. It was realized with materials and dimensions as given in Section 2.6 and Fig. 3f. All mu-metal components have been annealed accurately after machining. The results are as follows: The residual azimuthal inhomogeneity of the magnetic field was found to be zero within experimental uncertainty, indicating any local remanent magnetization of the field shaping shell or the pole faces to be insignificant. Shimming towards optimal field homogeneity was accomplished by wrapping four layers of mu-metal foils around the upper and the lower parts of the field shaping shell. This increased its total thickness towards its front ends in four steps by 0.1 mm, 0.1 mm, 0.1 mm and 0.05 mm, respectively at distances of z equals ±70 mm, ±60 mm, ±45 mm and ±40 mm from the respective shell edge. These numbers are in fair agreement with those found in the simulation.

Fig. 6a shows three scans of the axial field component B_z taken parallel to the central z-axis at distances of $x = 19.5$ cm (squares and dots) and $x = 13$ cm (triangles), respectively. The former are lying close to the field shaping shell and hence represent the tangential field (7) at its surface fairly well. We recognize that on the way to the central plane at $z = 0$, before shimming the field drops by more than 50% (squares) due to the strong stray flux out of the rather saturated shell. Stepwise shimming compensates this central depression, but with a rather deep modulation left over which might be reduced by adding more and finer steps. Anyway, this modulation dies out quite fast towards the axis (see also Fig. 3f). At $x = 13$ cm (triangles) it cannot be recognized any more. In Fig. 6b the decisive relative field gradient (2) has been plotted, measured along a diameter close to the central plane. It shows a broad central plateau with $\boldsymbol{G}_{\perp\mathrm{rel}} < 10^{-3}/\mathrm{cm}$, followed by a steep rise at large radii. Criterion (4) is fulfilled within a radius of 15 cm which corresponds to a filling factor of $F = 50\%$. Three of our 1.1 liter ^{3}He-flasks fit into this space (see Fig. 1).[7]

The gradient relaxation time in mark 3 was measured as described for mark 2. The result $T_{1G} \approx 403(67)$ h falls into the expected range. The measurement of the shielding factors yielded $S_{\uparrow\uparrow} = 6.5$ and $S_{\perp} = 179$, respectively. It is noteworthy that this latter maneuver did not leave any trace of remanent shift or deterioration of the field inside the box, contrary to the experience with mark 2.

When a spin box is opened for loading/unloading, the field gradient rises strongly (in particular near its sharp rim) – a fact which disfavors lengthy maneuvers. Leaving spin box mark 3 open as shown in Fig. 1, the relaxation time in a flask inside was found to drop down to about a quarter of an hour at the usual ^{3}He-pressure of 2.7 bar.

4. Magnetic fields inside shielded solenoids

Solenoids and Helmholtz coils are the most popular standard solutions for generating homogeneous magnetic fields within large volumes, because they are easy to build. Still the field on the axis of the latter, for instance, drops already by 5% on the way from the centre to the planes of the two coils which are separated from each other by a distance equal to the coil radius. At the same aspect ratio, the field of a non-shimmed solenoid drops even faster. But it is known that this drop can be removed by tightly covering the solenoid with flat pole faces from soft-magnetic material which are connected by a yoke as a magnetic short circuit as sketched in Fig. 7 by a longitudinal cross-section.

At very high permeability of pole faces and yoke, the loop integral over the field H around the total number N of windings, carrying the current I, is practically reduced to the path along the constant length L in-between the pole faces. From this follows H being constant inside:

$$H = (1/L)\oint \mathbf{H}\mathrm{d}\mathbf{s} = N\,I/L = \mathrm{const.} \qquad (10)$$

We may also interpret the short circuited pole faces as a pair of magnetic mirrors which mirror the solenoid current forth and back, thus simulating an infinitely long solenoid which also yields (10). The shape of the transverse cross-section of the solenoid does not

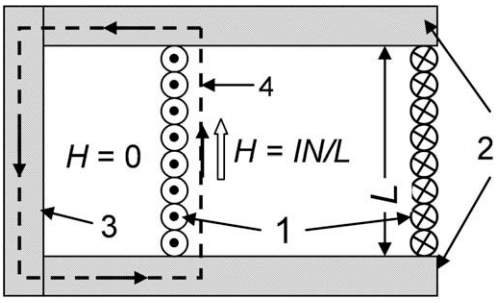

Fig. 7. Cross-section of a solenoid **1** covered by pole faces **2** which are short circuited by a yoke **3**; **4** = path of the loop integral according Eq. (10).

[7] Spin box mark 3 is now commercially available from Sekels GmbH, Ober-Mörlen, Germany [http://www.sekels.com].

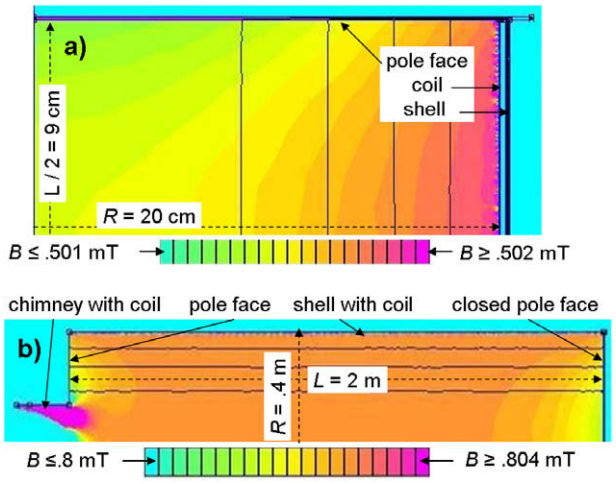

Fig. 8. (a) Simulation of the magnetic field in a small, shielded solenoid serving as a spin box for shipping polarized ^{3}He. Shown is one quadrant of the cross-section. (b) Simulation of the magnetic field in a large, shielded solenoid with an opening in the left pole face. Shown is the upper half of a longitudinal cross-section.

matter; it may be circular or rectangular or whatever. Neither does the shape of the yoke matter as long as it short circuits the magnetic flux between the pole faces properly. It is only for shielding purposes that we like it to fully enclose the solenoid. In the following we will conceive various configurations of shielded homogeneous magnetic field sources on this basis.

4.1. Simple case of a uniaxial, shielded solenoid

First we discuss a simple uniaxial solenoid which fits tightly into a box from mu-metal. The transverse cross-section is assumed to be circular, which allows for a fast 2D numerical field simulation using *femm 4.0*. Since this device may serve as a spin box for storage and transport of hyperpolarized ^{3}He we have chosen the dimensions $R = 20$ *cm*, $L = 18$ cm, similar to those given in Fig. 3. The solenoid is powered by a current density $j = N\,I/L$ of 400 Ampere windings per meter which yields a magnetic field of $B_0 = 0.5$ mT inside. The mu-metal sheets are 1.5 mm thick, enough to provide excellent shielding and to carry the flux of 0.6 Tcm^2 from the solenoid with little stray flux. Fig. 8a shows the simulated magnetic field distribution in a quadrant of the box with a step grading of the false color plot of $\Delta B/B_0 = 10^{-4}$. The relative field gradient is apparently in the range of 10^{-4}/cm within the entire box. Thus criterion (4) is met without any shimming.

4.2. Correction of field defects due to missing windings and openings

Missing windings: In reality the design of a spin box will deviate from the simulated one in Fig. 8a in so far as there will be a small gap between the solenoid and the pole faces for insulation and protection which might be in the order of one winding out of *N*. Viewing the pole faces as magnetic mirrors, any slit between them and the solenoid would appear as a periodic vacancy in the windings; it would disturb the homogeneity of the field and hence has to be avoided. One may prove and check by simulation that this vacancy causes a relative field drop along the axis towards the pole faces in the order of $L/(R\,N)$. This still matters at typical numbers $N \approx 10^3$ and realistic aspect ratios $L/R \approx 1$. Hence these outermost windings must not be omitted but have to be shifted beneath their next neighbors, for instance. The relative field change caused by this tiny displacement is then of order $(L/RN)^2$ and hence negligible. If the solenoid is coiled discontinuously with spacing d between the current loops, one simply provides for a distance $d/2$ from the pole faces at the ends in order to continue the mirrored current loops at regular spacing.

Openings: Contrary to the hermetically closed spin boxes for mere transport purposes, a shielded solenoid in a laboratory setup will usually require some open access during operation. In the following paragraphs we will present two different solutions for correcting the magnetic field defects caused by such openings. The first uses the simple recipe of the previous paragraph again, namely shifting aside the interfering windings. Let us consider, for example, a circular opening with radius R in an (x, z)-side face of a solenoid, possessing a rectangular cross-section in the (x, y)-plane (see Fig. 9a). Windings hitting the opening are diverted symmetrically to the right and left along the rim until downstream they have reached their original z-position again. The undisturbed windings may be represented for simplicity by a continuous and constant current density $j = I\,(\Delta N/\Delta z)$ which would yield the constant field $H_0 = j$ inside like in (10). In the chosen configuration, however, the field fraction at a point P

$$H_{\mathrm{op}}(P) = \int_{\mathrm{opening}} \frac{(\vec{j}\times\vec{r}')}{4\pi r'^3}\,\mathrm{d}A, \tag{11}$$

which would stem from the opening according to the Biot–Savart equation is replaced by the field

$$H_{\mathrm{rim}}(P) = \int_{\mathrm{rim}} \frac{(\vec{I}_{\mathrm{rim}}\times\vec{r})}{4\pi r^3}\,\mathrm{d}s, \tag{12}$$

due to the rim current I_{rim}. Let us check the relative change of the field at a point P_0 on the axis of the opening in a distance d. The calculation yields

$$\frac{H_{\mathrm{rim}}(P_0) - H_{\mathrm{op}}(P_0)}{H_0} = \frac{(R/d)^2}{4(1+(R/d)^2)^{3/2}} - \left(\frac{1}{2} - \frac{1}{2\sqrt{1+(R/d)^2}}\right) \underset{R\ll d}{\rightarrow} -\frac{3}{16}\left(\frac{R}{d}\right)^4 + O\left(\frac{R}{d}\right)^6, \tag{13}$$

decaying like a quadrupole field at large distances. At $R/d < 0.3$ the relative field change (13) falls already below the 10^{-3} level. The shielded tri-axial solenoid described in Section 5.1 features this kind of design.

If one aims at a homogeneous field in the close vicinity of the opening as well, one may bend the crossing windings outwards along a chimney from soft-magnetic material, pointing in y-direction as shown in Fig. 9b. In the case of a circular cross-section of the chimney, for example, one generates a longitudinal current density on its inner surface this way which varies along the azimuth as

$$j(\varphi) = j(\varphi = 0)\cos\varphi = I\,(\Delta N/\Delta z)\cos\varphi. \tag{14}$$

In the case of a sufficiently long cylinder, this current distribution is well known to produce inside a constant field $H = I(\Delta N/\Delta z)$ in z-direction, just the same as the solenoid. In fact, this principle works independent of the particular shape of the cross-section of the chimney. This may be seen from a loop integral like (10) whose path crosses the chimney in z-direction over a distance l_z and is closed inside the chimney (Fig. 9b). By principle of construction, the enclosed number of windings increases in proportion to l_z and hence the loop integral. This already proves the above statement, because the high permeability of the chimney short circuits any other contribution. The currents running forth and back through the chimney may be closed outside on top of the shielding. It is not known to us whether such interlaced, shielded current configurations for continuing a homogeneous magnetic field into an opening, or into a channel connecting to a neighboring field volume have been realized yet. In the present problem, a tightly fitting shielding is important in order to short-circuit field lines outside the enclosed volume.

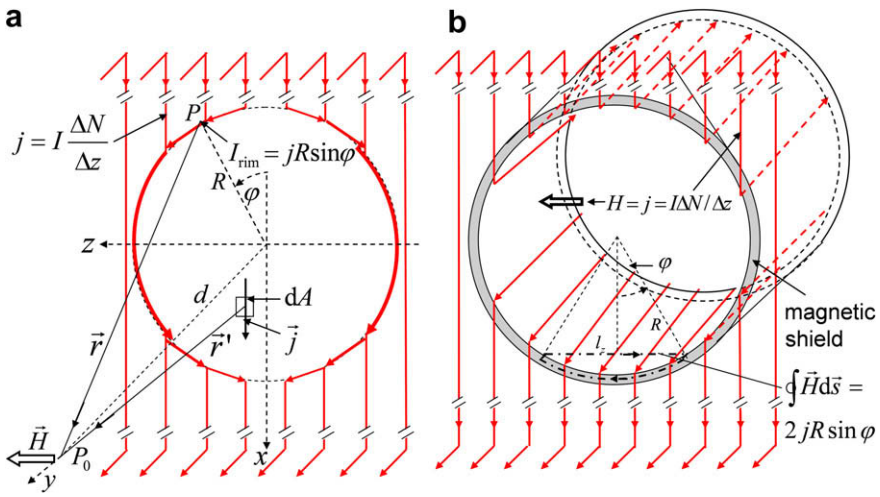

Fig. 9. Two schemes of correcting the magnetic field defect caused by a circular opening in a rectangular solenoid. (a) Diverting the concerned windings along the rim, (b) bending them outwards along the inner surface of a magnetic shielding tube. The rectangular magnetic shielding box which jackets the solenoid has been omitted in both cases.

The method works as well in the axial direction of a shielded solenoid. In this case one just continues the solenoid with the same current density into a magnetic shielding chimney which is attached to the respective bore in the pole face. With the bore on the axis, the problem can be simulated in 2D by *femm 4.0*. Fig. 8b shows the resulting field map for a large, shielded solenoid, 2 m in length and 0.8 m in diameter. The opening in one of the pole faces is 30 cm wide and covered by a 20 cm long chimney. A few extra windings at the open end of the chimney provide fine tuning of the field homogeneity close to the opening. Hence a surprisingly short aspect ratio of the chimney of only 2/3 suffices to limit the relative field gradient inside the main box to the level of 10^{-4}/cm. Shell, pole faces, and chimney are assumed to consist of 1.5 mm thick mu-metal sheets. This device is presently under construction at Sekels GmbH, Ober-Mörlen, Germany and will house a high performance ^{3}He-polarizer based on design principles of its forerunners [32,34,35].

5. Realization of current powered magnetic field boxes

In the previous theory section we confined the discussion to cases of a fixed field axis, but the principles work as well in tri-axial configurations allowing for a free choice of the field axis. Following the experimental development chronologically, we will present here first the realization of this more complex, but for our experiments indispensable tri-axial case. We will then turn to a brief discussion of the simple uniaxial spin box which has been realized only recently according to the simulation presented in Fig. 8a.

5.1. Shielded tri-axial solenoid with easy access

The device discussed in this section concerns the guiding field for a polarized ^{3}He target which has been in use for a decade by now for various scattering experiments at the electron beam of the MAMI accelerator at Mainz [6,36,37]. Details about the target itself and its operation (usually at a pressure of 5 bar) have been published separately [38]. The target is surrounded by up to three detectors close by, two of them being magnetic spectrometers. The latter cause stray fields of 0.2 mT around the target, forming a relative gradient of about 0.015/cm, far above the aspired limit of 10^{-3}/cm. The layout is sketched in Fig. 10. The particular challenge was to provide at the 20 cm long and 10 cm wide target a shielded, homogeneous holding field for the polarized spins which can be turned with high precision into any desired direction during operation. Moreover, permanent openings were required for entering and exiting of the electron beam and two more for detecting charged scattered particles under sizeable solid angles by the magnetic spectrometers. Similar situations are met in many other physics experiments. In free laboratory space this task is usually met by three pairs of orthogonal Helmholtz coils. But they would have required dimensions which would not have fit into the given setup. Moreover the stray field and the iron of the spectrometers would have spoiled the field produced by any unshielded current coils.

It turned out that a set of three orthogonal solenoids, tightly fitted into a rectangular magnetic shielding box, can meet the demands. For each of the three axes, two opposite walls of the shielding box serve as pole faces alternately, whereas the other four form the yoke for returning the flux. It is clear from the conception and calculations in Section 4 that such configurations can yield a quite homogenous magnetic field within the entire enclosed volume. In Section 4.2 we also presented two different solutions how field defects due to the necessary openings may be minimized. Here the demands could be fulfilled by choosing the simpler, though less accurate one, namely diverting the interfering windings around the rim of the opening.

But how to enable easy access to the enclosed target which has to be exchanged twice a day for a freshly polarized one? This problem has been solved as follows: The current loops are not closed inside the box, but spooled around each of its six walls and for each in both orthogonal directions (see insert in Fig. 10). Mounted together, they form three orthogonal sets, each powered by the same current, oriented such that any current which leaves the box along a wire at one edge of a wall is replaced by the same current entering through another wire at the bordering edge of the neighboring wall. Hence they form quasi closed current loops along the inner and outer box surface providing three orthogonal quasi solenoids inside and outside with opposite current sense. The inner ones supply a homogeneous magnetic field of any desired direction whereas the flux from the outer ones is shielded off by the soft-magnetic walls of the box. Access to the target is now possible just by lifting the top wall together with its two coils spooled around.

In the actual setup the mu-metal shield is surrounded by an outer pre-shield built from six iron plates separated from the inner shield by 10 mm thick PVC plates. Some details of the construction may be caught from the insert in Fig. 10. The windings enfold the inner and

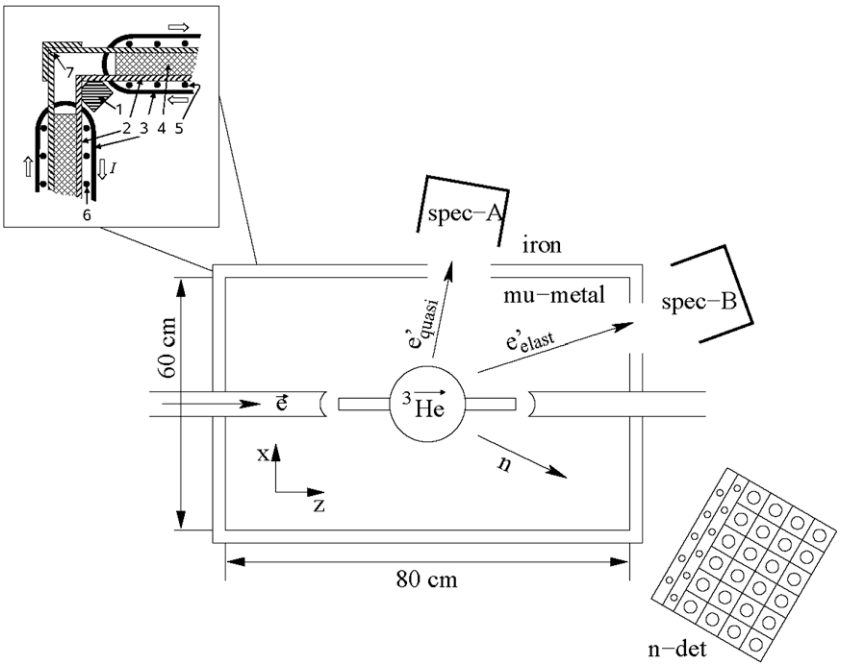

Fig. 10. Polarized ^{3}He target, set up at the Mainz Microtron accelerator (MAMI). The insert shows a detailed (x, z)-cross-section at one edge of the shielded tri-axial solenoid providing the magnetic holding field: (1) soft iron bar, (2) mu-metal shield, (3) B_y-coils, (4) PVC plate, (5) B_z-coil, (6) B_x-coil, (7) iron shield.

outer shielding plates. In order to allow for a good magnetic contact between bordering plates, their edges feature slits at a period of 10 mm into which the wire is pulled. The free margins can then be brought into tight magnetic contact. For the inner mu-metal plates this is accomplished by soft iron bars on which they rest; the outer iron plates are connected by iron angle profiles. The dimensions of the box are $60 \times 60 \times 80\ \mathrm{cm}^3$; the iron and mu-metal plates are 2 mm thick. The box is supported by an inner frame of aluminum bars. For both shields together, a shielding factor close to 50 has been measured which is sufficient. At the selected small field value of 0.4 mT the additional iron shield might be counterproductive, in fact, due to some uncontrolled remanent magnetization.

As already mentioned, the homogeneity of the field inside is affected by the necessary openings, namely the circular, 5 cm wide inlet and outlet holes for the accelerator beam, and in particular by the 12 cm wide and 5 cm high holes in front of the two spectrometers. The effect of the openings is twofold:

(i) Diverting of the interfering wires along the rim of the openings (see Fig. 9a) causes a relative field change inside given by (13) on its axis. In the case of a non circular cross-section one may replace R^2 in (13) by the area of the opening over π for simplicity. Inserting numbers, one realizes the relative field change at the site of the target to be in the order of 10^{-4} and hence negligible in the present application.
(ii) An external stray field B_e penetrates into the box and decays along the distance d from the window according to [39]

$$B(d) = B_e \exp(-k_{l(t)} d/D), \tag{15}$$

where D is the diameter (or diagonal) of the opening and $k_{l(t)} = 2.41(3.81)$ for the longitudinal (transverse) field component, respectively. This effect is only felt on the part of the wide windows exposed to the enhanced stray field from the two magnetic spectrometers facing them. But it turned out to be tolerable and did not require counteractions.

Still one observes a general, considerable decrease of all three magnetic field components towards their respective pole faces.

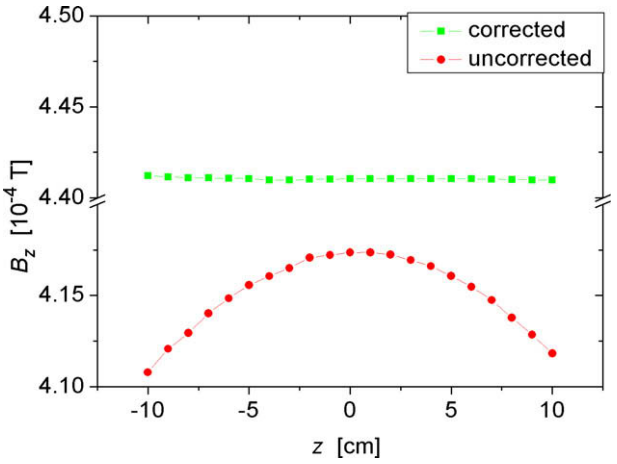

Fig. 11. z-component of the magnetic field in the center of the shielded, tri-axial solenoid before (circles) and after (squares) correction for missing windings at the margins of the box. The errors are dominated by inaccurate positioning of the sensor (approx. 2 mm). The lines between the symbols are guides for the eyes only.

This is shown for the z-component along the target axis by the circles in Fig. 11. The effect is clearly due to missing windings (compare Section 4.2) at the free margins of the internal shield (see insert of Fig. 10). As shown by the squares in Fig. 11, the decrease could be removed entirely by correction coils, each fixed to one of the inner surfaces of the mu-metal shield nearby the margins. The corrected field is constant over the full length of the target on the level of 10^{-4} and the field gradient is practically zero within measuring uncertainty. The high homogeneity of the field implies also that it can be turned into any desired direction by the respective choice of coil currents with high accuracy. This has been verified on the level of $\pm 0.3^\circ$.

In retrospect, the performance of this first realization of a shielded, tri-axial solenoid has turned out surpassing markedly the original demands; probably a considerably smaller, single shielded unit would have been even sufficient.

5.2. Uniaxial current powered spin box for transport purposes of polarized ^{3}He

The simplest configuration of a current powered, shielded field box is realized by fitting just a single solenoid into a cylindrical mu-metal box. The simulation presented in Fig. 8a has proven the high field homogeneity it can provide within the entire enclosed volume. Hence it could work quite well as a spin box for shipping polarized ^{3}He, however with the handicap of carrying a battery along. Regarding size and weight (including the battery), it competes with the permanently magnetized spin boxes discussed above up to a field of about 1 mT. At higher fields the quadratic rise of power consumption starts causing inconveniences.

We realized this device with dimensions as given in Section 4.1. Both edges of the yoke are beaded outwards to form 10 mm wide, flat margins in order to assure magnetic contact to the pole faces. The bottom face is firmly screwed to the yoke, the top face is fixed by a clamp ring allowing a fast loading and unloading maneuver. The design looks quite similar to the one shown in Fig. 1. The solenoid consists of two layers of copper wire (0.4 mm in diameter), spooled onto a PVC bobbin. Although it fits tightly into the box, a 0.8 mm wide PVC safety margin separates the coil from the pole faces. In order to avoid a corresponding field decrease towards the pole faces, the missing windings are placed beneath the outermost windings instead. The coil is powered by eight NiMH-batteries in series, housed in the socket of the box. With a capacity of 4 Ah they provide a field of 0.4 mT for 40 h.

Fig. 12a shows four typical scans of the magnetic field in the closed box in axial direction, taken at radii $R = 0$ cm, 8 cm, 15 *cm*, *and* 17.5 *cm*, respectively. Except for an enhanced field drop in the very peripheral zones of the box, the measured field distribution reproduces the simulated one in Fig. 8a fairly well. Slight residual irregularities and asymmetries are to be seen, e.g. in the central pole face regions. They are probably due to mechanical imperfections which are likely to occur in such a light sheet construction. Fig. 12b shows the corresponding relative transverse field gradient as defined in (2). We recall from [1] that $R = 15$ cm marks about the borderline of the used storage volume within which $\boldsymbol{G}_{\perp\mathrm{rel}} \lesssim 10^{-3}/\mathrm{cm}$ is aspired. Except for two spots (which are actually not occupied by the ^{3}He-flasks), the results fall well below this limit. This has been confirmed by a measurement of the gradient relaxation time at a ^{3}He-pressure of 550 mbar yielding $T_{1\ \mathrm{grad}} = 165(40)$ h. According to (2), this result corresponds to an average of $\left\langle \boldsymbol{G}^2_{\perp\mathrm{rel}} \right\rangle^{1/2} = 7 \times 10^{-4}/\mathrm{cm}$, or likewise to $T_{1\ \mathrm{grad}} \approx 800$ h at the nominal pressure of 2.7 bar at which we usually ship polarized ^{3}He. In view of this satisfactory result further improvements of the field homogeneity are superfluous. The shielding factor has been measured to be $S = 60$ in axial and $S = 600$ in radial direction. Both values are much higher than reported for the permanently magnetized boxes because the direct magnetic contact between the shield and the pole faces is not interrupted in this configuration. Still the axial shielding is weaker than the radial one due to the flat aspect ratio of the box.

In the lab and during transport by car the current powered spin box has functioned reliably, but during airfreight it has occasionally failed for unknown reasons, actually. Possibly the temperature sank below the range of reliable operation of the batteries during the flight. Although this problem might be curable, we decided to avoid the risk and since are only using permanently magnetized spin boxes for airfreight.

Also a group at Institut Laue-Langevin, Grenoble, France (ILL) has recently reported on a current powered spin box which is suited for local transport of polarized ^{3}He within the lab [33]. Following design principles described in Section 5.2, it concerns a rectangular mu-metal box. For reasons of convenience, however, it is fully open on two opposite sides like in the case of the permanently magnetized, so called "magic box" being also in use at ILL [33]. Coils are spooled around two of the walls, the other two serve as pole faces. The ^{3}He cell is stored in the central section which is sufficiently homogeneous and shielded due to an adequate choice of dimensions and aspect ratio.

6. Conclusions

In this paper we described various concepts and realizations of magnets providing a homogeneous magnetic field within a large fraction of volume inside a magnetic shield. The goal was achieved satisfactorily by permanent magnetic field sources and to a higher degree even by embedded solenoids. These developments were guided partly by the need of housing and shipping polarized gaseous spins, particularly ^{3}He, within shielded magnetized boxes featuring a low relative field gradient $\boldsymbol{G}_{\perp\mathrm{rel}} \lesssim 10^{-3}/\mathrm{cm}$ in order to suppress gradient relaxation. Since the absolute field value is hardly restricted, a comfortable region around 1 mT is preferred.

Regarding permanently magnetized boxes we realized solutions based on two new principles of homogenizing the magnetic field. The first starts from a pot-like magnet with the front ends serving as pole faces and the shell as a yoke. The strong radial decrease of the field inside is compensated by an optimized distribution of permanent magnets along the shell. The realized version (mark 1) fulfils the homogeneity criterion within roughly 30% of its total volume. Polarized ^{3}He has been shipped in such boxes since years

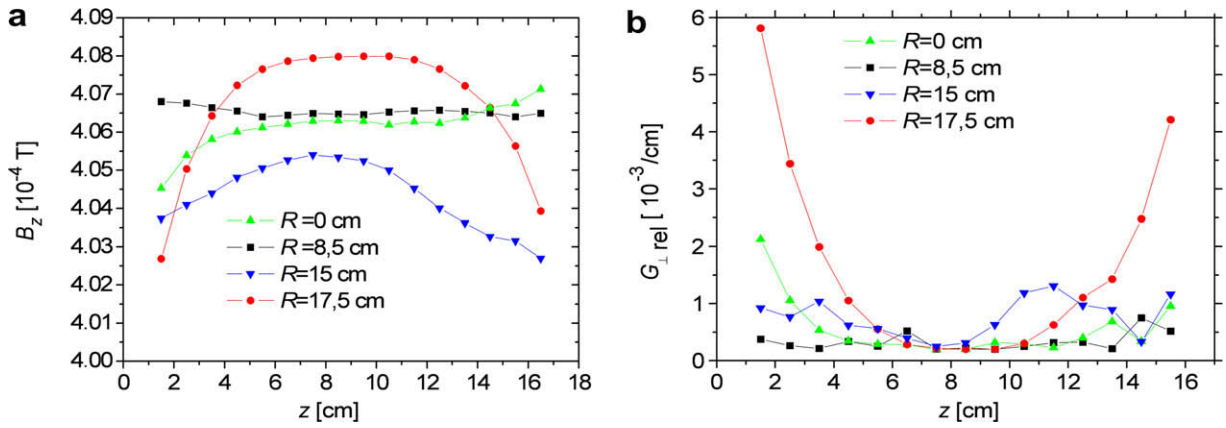

Fig. 12. Axial scans of the magnetic field (a) and the transverse relative field gradient (b) in a current powered spin box, taken at four different distances from the central axis. In both diagrams, the errors are dominated by inaccurate positioning of the sensor (approx. 2 mm). The lines between the symbols are guides for the eyes only.

by airfreight to different customers at MRI-facilities in particular for the purpose of lung imaging.

The second procedure has the capability of homogenizing virtually the entire enclosed volume to a high degree. It starts from the idea to enclose the space between two flat pole faces of a magnet with a (thin) shell from soft-ferromagnetic material which is magnetized parallel to the enclosed field with a constant tangential magnetizing field $H_{\uparrow\uparrow}$. The realization of this idea requires, however, compensating the stray flux out of the shell by a proper adjustment of the solid cross-section of this field shaping shell. Simulations confirm these ideas and find fairly simple configurations which fulfill the homogeneity criterion within up to 80% of the enclosed volume. According to this principle we have built two prototypes (mark 2 and mark 3) which differ in the design and in the choice of materials. After coarse shimming of the shell thickness, both designs have reached 50% of useful volume. Satisfactory performance requires low coercive field strength and proper annealing of the soft-magnetic materials used.

Homogenizing a magnetic field within large volumes by parallel shell magnetization seems generally possible up to magnetic fields of order 100 mT and may meet interesting applications. As examples, we have simulated – though not presented in this paper – configurations of permanently magnetized, compact, lightweight magnets at fields around 50 mT which could be quite useful in the upcoming area of low field tomography of hyperpolarized substances.

On the other hand, flexible laboratory solutions for homogeneous magnetic fields inside a shielding box can be provided quite generally and efficiently by fitting solenoids into the shield. We have realized in particular a tri-axial configuration which allows for a free and precise choice of field value and direction, even under conditions of external stray fields and of restricted space. Such current powered boxes allow also for topologies which provide free access through openings without deteriorating seriously the field homogeneity inside.

Comparing the homogenizing effect of a parallel magnetized field shaping shell to that of an inner solenoid enclosed in the shielding box, we recognize that both solutions aim at establishing the same boundary condition: At the inner lateral face of the box the magnetic field $B_{\mathrm{out}\uparrow\uparrow}$ should be constant and parallel to that in the centre. The field shaping shell achieves this by a constant, but (necessarily) rather saturated magnetization $B_{\mathrm{in}\uparrow\uparrow}$ which transmits a tiny tangential fraction $B_{\uparrow\uparrow\mathrm{out}} = B_{\uparrow\uparrow\mathrm{shell}}/\mu_{\mathrm{shell}}$ through its boundary into the box. In the case of the solenoid fitted into a flux returning yoke, the opposite but weaker and non-saturated yoke magnetization transmits (due to the higher μ yoke) a still tinier fraction into the box which is opposite to a much stronger solenoid field, resulting in : $B_{\uparrow\uparrow\mathrm{out}} = B_{\uparrow\uparrow\mathrm{solenoid}} - B_{\downarrow\downarrow\mathrm{yoke}}/\mu_{\mathrm{yoke}}$. Moreover, the fairly saturated field shaping shell is loosing a much stronger transverse stray flux into the box than the non-saturated yoke does. Therefore, the field shaping shell yields still unsatisfactory field homogeneity in the peripheral zone of the box whereas the embedded solenoid yields substantially smaller field gradients all over the enclosed volume.

We are using both types of devices as "spin boxes" in order to provide a small holding field up to 1 mT for spin-polarized ^{3}He. The permanently magnetized spin boxes serve for storing polarized ^{3}He as well as for shipping it worldwide. Current powered boxes are preferred in laboratory applications.

Acknowledgments

The authors are grateful to the personnel of the mechanical workshop of our institute for the elaborate manufacturing of the spin boxes. Authors and topics of this paper have been supported over the years by the Deutsche Forschungsgemeinschaft contracts # SFB 443 and FOR 474 HE 2308, by the Stiftung Rheinland-Pfalz für Innovation contract # 15202-38 62 61/539, by the European Union within projects PHIL, FP 5 contract # QLG1-2000-01559 and PHELINET, FP 6 ref. 36002 as well as by the European Space Agency (ESA), contract # 15308/01/NL/PA.

Appendix. . Relative magnetic field gradient in an axisymmetric saddle point field

Assuming axial symmetry, the gradient term in (2) transforms in cylindrical coordinates to

$$\boldsymbol{G}^2_{\perp\mathrm{rel}} = \frac{1}{B_0^2}\left(\left(\frac{\partial B_r}{\partial r}\right)^2 + \left(\frac{\partial B_r}{\partial z}\right)^2 + \left(\frac{B_r}{r}\right)^2\right), \tag{A1}$$

where r is the distance from the central field axis. Using the free field equations, reading now

$$\mathrm{div}\vec{B} = \frac{B_r}{r} + \frac{\partial B_r}{\partial r} + \frac{\partial B_z}{\partial z} = 0, \tag{A2}$$

and

$$\mathrm{rot}\vec{B} = \left(\frac{\partial B_r}{\partial z} - \frac{\partial B_z}{\partial r}\right)\hat{\varphi} = 0, \tag{A3}$$

we can replace the derivatives of the radial field B_r in (A1) by those of B_z and obtain

$$\boldsymbol{G}^2_{\perp\mathrm{rel}} = \frac{1}{B_0^2}\left(\left(\frac{\partial B_z}{\partial z} + \frac{B_r}{r}\right)^2 + \left(\frac{B_r}{r}\right)^2 + \left(\frac{\partial B_z}{\partial r}\right)^2\right). \tag{A4}$$

Any fairly optimized homogeneous magnetic field will show a saddle point of at least second or even higher order in its center which forms a flat central field plateau followed by steeply rising field gradients further out. Hence the term B_r/r may be neglected against the radial derivative $\partial B_r/\partial r$; this yields the first of the two approximations given in (2). Using an NMR probe rather than a vector magnetometer one measures the amount B instead B_z. Still we may write any derivative of B in terms of the derivative of B^2, furthermore make use of the assumptions $B \approx B_0 \approx B_z \gg B_x, B_y$ and obtain

$$\frac{\partial B}{\partial x_i} = \frac{1}{2B}\frac{\partial B^2}{\partial x_i} \approx \frac{B_x}{B_0}\frac{\partial B_x}{\partial x_i} + \frac{B_y}{B_0}\frac{\partial B_y}{\partial x_i} + \frac{B_z}{B_0}\frac{\partial B_z}{\partial x_i} \approx \frac{\partial B_z}{\partial x_i}. \tag{A5}$$

Hence we may replace B_z by B in the final results (A4) and (2).

References

[1] J. Schmiedeskamp, W. Heil, E.W. Otten, R.K. Kremer, A. Simon, J. Zimmer, Eur. Phys. J. D 38 (2006) 427.
[2] T.G. Walker, W. Happer, Rev. Mod. Phys. 69 (1997) 629.
[3] S.R. Parnell, E. Babcock, K. Nünighoff, M.W.A. Skoda, S. Boag, S. Masalovich, W.C. Chen, R. Georgii, J.M. Wild, C.D. Frost, Nucl. Instrum. Methods A 598 (2009) 774.
[4] P.-J. Nacher, M. Leduc, J. Phys. (Paris) 46 (1985) 2057.
[5] R. Surkau, J. Becker, M. Ebert, T. Großmann, W. Heil, D. Hofmann, H. Humblot, M. Leduc, E.W. Otten, D. Rohe, K. Siemensmeyer, M. Steiner, F. Tasset, N. Trautmann, Nucl. Instrum. Methods A 384 (1997) 444.
[6] D. Rohe, P. Bartsch, D. Baumann, et al., Phys. Rev. Lett. 83 (1999) 425.
[7] G.L. Jones, T.R. Gentile, A.K. Thompson, Z. Chowdhuri, M.S. Dewey, W.M. Snow, F.E. Wietfeldt, Nucl. Instrum. Methods A 440 (2000) 772.
[8] W. Heil, K.H. Andersen, R. Cywinski, H. Humblot, C. Ritter, T.W. Roberts, J.R. Stewart, Nucl. Instrum. Methods A 485 (2002) 551.
[9] M.S. Albert, G.D. Cates, B. Driehus, W. Happer, B. Saam, C.S. Springer, A. Wishnia, Nature 137 (1994) 199.
[10] M. Ebert, T. Großmann, W. Heil, E.W. Otten, R. Surkau, M. Leduc, P. Bachert, M.V. Knopp, L.R. Schad, M. Thelen, Lancet 347 (1996) 1297.
[11] For a brief survey see e.g.: E.W. Otten, Europhys. News 35 (1) (2004) 16.
[12] J.M. Wild, J. Schmiedeskamp, M.N.J. Paley, F. Filbir, S. Fichele, L. Kasubosky, F. Knitz, N. Woodhouse, A. Swift, W. Heil, G.H. Mills, M. Wolf, P.D. Griffiths, E.W. Otten, E. van Beek, Phys. Med. Biol. 47 (2002) N185.
[13] F. Thien, M. Friese, G. Cowin, D. Mailet, D. Wang, G. Galloway, I. Brereton, P.J. Robinson, W. Heil, B. Thompson, Respirolo 13 (2008) 599.
[14] L.D. Schearer, G.K. Walters, Phys. Rev. 139 (1965) A1398.
[15] R. Barbé, M. Leduc, F. Laloe, J. Phys. 35 (1974) 699.

[16] V. Lefèvre-Seguin, P.-J. Nacher, F. Laloe, J. Phys. 43 (1982) 737.
[17] G.D. Cates, S.R. Schaefer, W. Happer, Phys. Rev. A 37 (1988) 2887.
[18] R. Barbé, M. Leduc, F. Laloe, J. Phys. 35 (1974) 935.
[19] N.R. Newbury, A.S. Barton, G.D. Cates, W. Happer, H. Middleton, Phys. Rev. A 48 (1993) 4411.
[20] J. Schmiedeskamp, H.-J. Elmers, W. Heil, E.W. Otten, Yu. Sobolev, W. Kilian, H. Rinneberg, T. Sander-Thoemmes, F. Seifert, J. Zimmer, Eur. Phys. J. D 38 (2006) 445.
[21] E.W. Otten, E. Aidam, M. Ebert, T. Großmann, W. Heil, D. Rohe, R. Surkau, Patent Nr. DE 19742548 C2, Deutsches Patent- und Markenamt and PCT/EP98/06056, 1998.
[22] S. Hiebel, Doctoral thesis, Mainz University, 2006.
[23] E.W. Otten, S. Hiebel, W. Heil, J. Schmiedeskamp, Offenlegungsschrift DE 10 2006 055 559 A1, Deutsches Patent- und Markenamt.
[24] Datasheet by Koenig Feinstahl AG, CH-8953 Dietikon, Switzerland, 2005.
[25] Magnetische Abschirmungen, Vacuumschmelze Hanau, Germany, 1988.
[26] Catalogue by comp. IBS Magnet, Berlin, Germany, 1999.
[27] Technische Tabellen, Siemens AG, Germany, 1987.
[28] For specifications see: <http://www.magnetsysteme.de>.
[29] <http://www.phil.ens.fr>.
[30] <http://www.phelinet.eu>.
[31] T. Großmann, Doctoral thesis, Mainz University, 2000.
[32] J. Schmiedeskamp, Doctoral thesis, Mainz University, 2004.
[33] A.K. Petoukhov, V. Guillard, K.H. Andersen, E. Bourgeat-Lami, R. Chung, H. Humblot, D. Jullien, E. Lelievre-Berna, T. Soldner, F. Tasset, M. Thomas, Nucl. Instrum. Methods A 560 (2006) 480.
[34] M. Ebert, Doctoral thesis, Mainz University, 2000.
[35] A. Deninger, M. Ebert, J. Hasse, W. Heil, E.W. Otten, J. Schmiedeskamp, R. Surkau, Patent Nos. DE 100 00 675, 2000 and [US] 09/758,006, 2001.
[36] Daniela Rohe, Doctoral thesis, Mainz University, 1998.
[37] C. Carasco et al., Phys. Lett. B 559 (2003) 41–48.
[38] J. Krimmer, M. Distler, W. Heil, S. Karpuk, D. Kiselev, Z. Salhi, E.W. Otten, Nucl. Instrum. Methods A 611 (2009) 18.
[39] A. Mager, Z. Angew. Phys. 381 (1967) 23.